Journal of Electrochemical Science and Technology
Vol. 4, No. 2, 2013, 71-80
http://dx.doi.org/10.5229/JECST.2013.4.2.71

THE KOREAN ELECTROCHEMICAL SOCIETY **Journal of Electrochemical Science and Technology**

Methyl Viologen Mediated Oxygen Reduction in Ethanol Solvent: the Electrocatalytic Reactivity of the Radical Cation

Qianqi Lin, Qian Li, Christopher Batchelor-McAuley, and Richard G. Compton*
Department of Chemistry, Physical and Theoretical Chemistry Laboratory, Oxford University, South Parks Road, Oxford OX1 3QZ, United Kingdom

Abstract:

The study of methyl viologen (MV^{2+}) mediated oxygen reduction in electrolytic ethanol media possesses potential application in the electrochemical synthesis of hydrogen peroxide mainly due to the advantages of the much increased solubility of molecular oxygen (O_2) and high degree of reversibility of $MV^{2+/\bullet+}$ redox couple. The diffusion coefficients of both MV^{2+} and O_2 were investigated via electrochemical techniques. For the first time, MV^{2+} mediated O_2 reduction in electrolytic ethanol solution has been proved to be feasible on both boron-doped diamond and micro-carbon disc electrodes. The electrocatalytic response is demonstrated to be due to the radical cation, $MV^{\bullet+}$. The homogeneous electron transfer step is suggested to be the rate determining step with a rate constant of $(1 \pm 0.1) \times 10^5$ $M^{-1}s^{-1}$. With the aid of a simulation program describing the EC' mechanism, by increasing the concentration ratio of MV^{2+} to O_2 electrochemical catalysis can be switched from a partial to a 'total catalysis' regime.

Keywords: Methyl viologen, mediated oxygen reduction, ethanolic solution, diffusion coefficient and concentration of oxygen, homogeneous rate constant

Received June 7, 2013 : Accepted June 17, 2013

1. Introduction

Methyl viologen (or 1,1'-dimethyl-4,4'-bipyridinium dichloride or paraquat) has been studied as a redox mediator in biological systems and as a component for LEDs and LCDs due to marked colour difference between its oxidation states.[1-3] As shown in Scheme 1, methyl viologen exhibits three major states, *viz.* MV^{2+}, $MV^{\bullet+}$ and MV^0. Its electrochemical redox behaviour has been investigated in various electrolytic solvents, such as dimethyl sulfoxide, dimethylformamide, dichloromethane, etc. using hanging mercury drop, gold, platinum, glassy carbon, pyrolytic graphite carbon, boron-doped diamond electrodes.[2,4-6] In most cases, the rates of electron transfer for both the first and second reductions demonstrate fast kinetics.

*Corresponding author. Tel.: +44 (0) 1865 275413
E-mail address: richard.compton@chem.ox.ac.uk

Methyl viologen mediated reduction of oxygen (O_2) is of great importance in biology. Under physiological conditions, methyl viologen is known to be an effective and non-selective herbicide. Its herbicidal activity was found to be linked to the redox couple of $MV^{2+/\bullet+}$ possessing a low reduction potential and a high degree of electrochemical reversibility.[7-9] The related electrocatalytic (EC') mechanism can be described as

$$MV^{2+} + e^- \overset{k_0}{\leftrightarrow} MV^{\bullet+} \quad (1)$$

$$MV^{\bullet+} + O_2 \xrightarrow{k_f} MV^{2+} + O_2^{\bullet-} \quad (2)$$

where k_0 is the heterogeneous electron transfer rate constant (cm s^{-1}), and k_f is the homogeneous rate of electron transfer (mol^{-1} dm^3 s^{-1}). In the EC' mechanism, acts as the mediator to reduce O_2 to superoxide ($O_2^{\bullet-}$). The further reduced product resulting from this mediated process is hydrogen peroxide, which is an

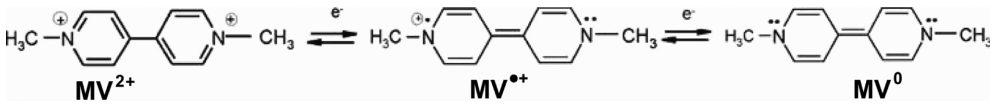

Scheme. 1. Structures of three oxidation states of methyl viologen.

industrially important compound.[10,11] Beyond industrial production of hydrogen peroxide, small scale synthesis of dilute peroxide solutions (3~8 %) at the point of use can be somewhat desirable in applications such as sterilisers, peroxide-based hair dyes, chlorine-free bleach etc.[12] Hence, methyl viologen mediated oxygen reduction poses potential application in chemical synthesis for hydrogen peroxide. Usually, the low solubility of oxygen in aqueous systems has posed a limitation to the final turnover of the sought hydrogen peroxide product. Organic solvents, such as acetonitrile, dimethyl sulfoxide, dimethylformamide and ethanol, are known to have much higher oxygen solubility.[13] Hence, within the present work, ethanol was used as the reaction solvent to study the methyl viologen mediated oxygen reduction. Chronoamperometry was used to independently determine the precise values of the diffusion coefficient and solubility of oxygen in the electrolytic ethanol solution. Prior to the further investigation of the electrocatalytic process, methyl viologen was studied in the absence of oxygen allowing the heterogeneous rate of electron transfer to be obtained *via* simulation. For the first time methyl viologen mediated oxygen reduction in ethanol is shown to be feasible on both boron-doped diamond electrodes and carbon micro-disc electrodes. In contrast, no electrocatalytic behaviour is shown in aqueous solution on carbon micro-disc electrodes within this work. The resulting electrocatalytic steady-state currents were successfully modelled for both air-equilibrated and oxygen-saturated conditions. The obtained homogeneous rate constant, k_f, was estimated to be $(1 \pm 0.1) \times 10^5$ $M^{-1}s^{-1}$. A potential dependent electrocatalytic steady-state current is proposed to be related to the migration current contribution, which is arguably useful due to the extra enhancement to mass transport upon diffusion in electrocatalytic oxygen reduction.

2. Experimental section

2.1 Chemical reagents

All chemicals were purchased from Sigma-Aldrich at the analytical grade and used without any further purification. These were methyl viologen dichloride hydrate ($C_{12}H_{14}Cl_2N_2{\cdot}3H_2O$), tetra-*n*-butylammonium chloride (TBACl), ferrocene (Fc) and tetra-*n*-butylammonium perchlorate (TBAP). All solutions were prepared by using ethanol (EtOH) in the purity of over 99.8%.

2.2 Equipment

An Autolab PGSTAT20 computer controlled potentiostat (EcoChemie, Utrecht, The Netherlands) was used to perform electrochemical measurements. A standard three-electrode configuration was used throughout. The working electrode was a macro-boron doped diamond electrode (macro-BDD, 3.0 mm diameter, Windsor Scientific, Slough, U.K.), or a micro-carbon fibre electrode (μ-C, calibrated radius, r_d, of 4.17 μm, BASi, MF-2007). The cell assembly was completed by using a platinum wire (99.99%, 0.5 mm diameter, GoodFellow, Cambridge, UK) acting as the counter electrode, and a reference electrode being a 0.5 mm diameter silver wire or a leakless Ag/AgCl (1 M KCl aqueous solution) reference electrode (eDAQ, ET072), or a standard calomel electrode (SCE). The radius (r_d) of the working micro-electrode was calibrated by analyzing the steady-state current of a 2 mM ferrocene solution in anhydrous acetonitrile with 0.1 M TBAP as supporting electrolyte at 298.0 K. A literature diffusion coefficient of 2.43×10^{-9} $m^2 s^{-1}$ at 298.0 K was adopted[14] to determine the radius, r_d, by using the following equation:[15]

$$I_{ss} = 4nFDCr_d \quad (3)$$

where I_{ss} is the steady-state limiting current, n is the number of electrons transferred, F is the Faraday constant, D is the diffusion coefficient (cm^2 s^{-1}), C is the bulk concentration of the electroactive species (mol dm^{-3}) and r_d is the radius of the electrode. The macro-BDD and μ-C electrodes were polished with diamond spray of decreasing particle sizes (3.0 mm, 0.1 mm, 0.01 mm, Kemet Ltd., UK. After sonicating in EtOH for one minute, the working electrode was dried completely by blowing nitrogen over the surface before immersing it into the reaction solution. All experiments were carried

out in a water bath at (298 ± 0.5) K within a Faraday cage to minimise background electrical noise.

2.3 Single potential step chronoamperometry

Single potential step chronoamperometry, due to the varying influence of both spherical and planar diffusion at a microdisc electrode over the experimental timescale, may be exploited to allow independent deconvolution of both the diffusion coefficient and solubility of the electroactive species from a single transient.[16-18] The analysis is based only on the knowledge of a disk electrode radius and the number of electrons transferred. The experiments were undertaken using a sample time of 0.001 s. Prior to the potential step the system was pretreated by holding a potential at which no faradic current was passed for 2 s, after which the current transient was obtained by stepping to a potential corresponding to the transport limited reduction of oxygen (at – 1.25 V) and held for 0.5 s. Note that data collected at the first 10 ms were discarded due to extensive double layer charging. The time-dependent current response obtained was then analysed by either a nonlinear fitting function in OriginPro 8.5.1 (Microcal Software Inc.) or a computational program described by Xiong *et al.*[17] The analysis was based on the following equation, as first proposed by Shoup and Szabo,[19] which describes the current response, I, over the entire time domain, with a maximum error of less than 0.5%.

$$I = 4nFDCr_d f(\tau) \quad (4)$$

where $f(\tau) = 0.7854 + 0.8863\ \tau^{-1/2} + 0.2146\ exp\ (-0.7823\ \tau^{-1/2})$ (5)

$f(\tau)$ is a τ dependent function, where τ is a dimensionless time (t) parameter, defined as $\tau = 4Dt/r_d^2$. Consequently, D and nC can be measured independently and simultaneously from the best-fit data to a potential step transient.

The numerical simulation to derive the heterogeneous electron transfer kinetic parameters was developed by Klymenko *et al.* and is based on two dimensional mass transport equations.[20] Both wave shape and steady-state current were fitted with experimental data. The simulated voltammograms were performed at a grid size of $N\Theta \times N\Gamma = 200 \times 200$ (where Θ and Γ are the transformed grid coordinates), and the time grid expansion parameter, Nt, of being 3000. These parameters are sufficient to achieve convergence error of less than 1%.

The numerical simulation to determine the homogeneous reaction kinetic parameters was developed by Ward *et al.*,[21] which simulates a simple electrocatalytic EC' mechanism at a microelectrode by coupling of the mass transport equations. After inputting the micro-disc radius (r_d), heterogeneous electron transfer kinetic parameters (k_0), diffusion coefficients (D) and concentrations (C) of the reactants, reductive current responses can be generated by adjusting the input homogeneous reaction rate constant (k_f), in order to fit the experimental voltammograms in terms of wave shape and magnitude.

The reaction solution was either saturated with nitrogen, air, or oxygen at atmospheric pressure as specified. All the experiments were repeated at least four times, and the errors are obtained from the standard deviation of all data points.

3. Results and discussion

This work first investigates the solubility and diffusion coefficient of oxygen (O_2) in anhydrous ethanol (EtOH) containing 0.1 M TBACl supporting electrolyte by using the mean scaled absolute deviation (MSAD) method based on Shoup and Szabo analysis.[19] Secondly, the electrochemical response of methyl viologen (MV^{2+}) in the absence of O_2 was studied to obtain the heterogeneous electron transfer kinetics. Finally the MV^{2+} mediated O_2 reduction is analysed and comparison is made to the same process in aqueous system. The homogeneous electrocatalytic pathways were studied with the aid of a simulation program. A potential dependent electrocatalytic steady-state current is then discussed.

3.1 Solubility and diffusion coefficient of O_2

The O_2 electrochemical redox response in an air-equilibrated anhydrous EtOH solution supported with 0.1 M tetra-*n*-butylammonium chloride (TBACl) was studied to obtain the solubility of oxygen (C_{O_2}) and diffusion coefficient of O_2 (D_{O_2}) using a carbon microdisc electrode (μ-C).

First, cyclic voltammograms were recorded at a scan rate of 25 mV s^{-1}, as shown in Fig. 1. The scan was ran from –0.5 V to –2.0 V (*vs.* Ag/AgCl–1 M KCl). The formal potential of $O_2/O_2^{\bullet -}$ ($E_{O_2/O_2^{\bullet -}}$) in EtOH has not been reported in the literature. However, a range of –0.825 V to –0.965 V (*vs.* Ag/AgCl–1 M

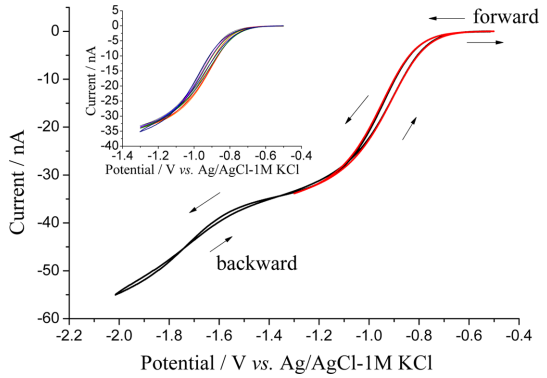

Fig. 1. Cyclic voltammogram for the direct O_2 reduction in an air-equilibrated EtOH/0.1 M TBACl solution on a μ-C electrode at 25 mV s^{-1} (black line). A repeated scan reversed at –1.3 V is overlapped in red, and its scan rate variation of 5, 10, 25, 50, 100, 200 and 1000 mV s^{-1} are shown in inset.

KCl) were previously reported in various other organic solvents.[22] At the potential range of *ca.* –1.2 V to –1.5 V, a steady-state current (I_{ss}) is achieved, corresponding to the reduction current of O_2. As the overpotential increases, further reduction is shown until it reaches solvent breakdown region beyond *ca.* –2.0 V. As can be seen in Fig. 1 the current crosses over at high overpotential; this likely suggests a change of the electrode surface resulting from attack by the formed reactive oxygen species. A voltammogram of same scan rate reversed at –1.3 V is also shown in Fig. 1, the inset of which illustrates scan rates variation from 5 to 1000 mV s^{-1}.

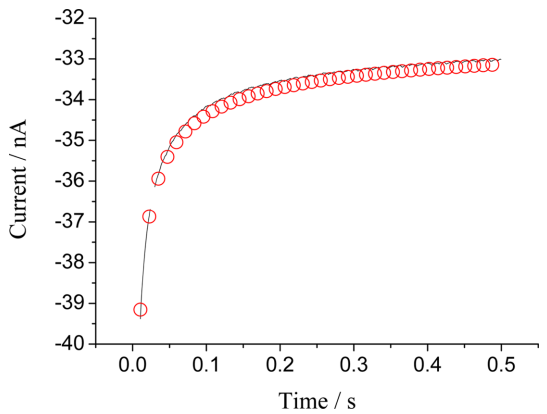

Fig. 2. The experimental (line) and simulated (circle) single potential step chronoamperometric transients for O_2 reduction in air-equilibrated EtOH/0.1 M TBACl solution on a μ-C electrode. The potential was stepped from 0 V to −1.25 V and back to 0 V *vs.* Ag/AgCl −1 M KCl leakless electrode.

Fig. 2 shows the chronoamperomogram obtained in the same reaction solution by stepping a potential from –0.5 V to –1.25 V (line). Single potential step chronoamperometry was performed as it can determine *nC* and *D* independently. The experimental procedure is described in Section 2.3. The experimental result can be analysed by using the Shoup and Szabo expressions (Eqn. (2)) to obtain the best-fit. In order to determine precise values of *nC* and *D*, the lowest mean scaled absolute deviation (MSAD) method can be used. The MSAD defines as the average error per point over the entire chronoamperometric transients.

$$\text{MSAD \%} = \frac{1}{N}\sum_{N}\left|\frac{I_{sim} - I_{exp}}{I_{exp}}\right| \times 100 \qquad (6)$$

where N is the number of experimental data points, I_{exp} is the experimental current and I_{sim} is the simulated current from Shoup and Szabo equation (Eqn. (2)).[17] This procedure can be computed and repeated by narrowing down the value ranges for *nC* (*n* is the number of electron transferred) and *D* for the same chronoamperomogram. Fig. 3 shows a two-dimensional contour plot of MSAD from the depicted chronoamperomogram in Fig. 2, where x and y axes correspond to *nC* and *D* respectively. The MSAD contour plot gives a minimum, as shown in Fig. 3. It can be seen that there are also a wide range of *nC* and *D* values that satisfy the fitting criteria of a maximum error of less than 0.5% (MSAD % < 0.5 %).

The final results of D_{O_2} and *n* × concentration of O_2

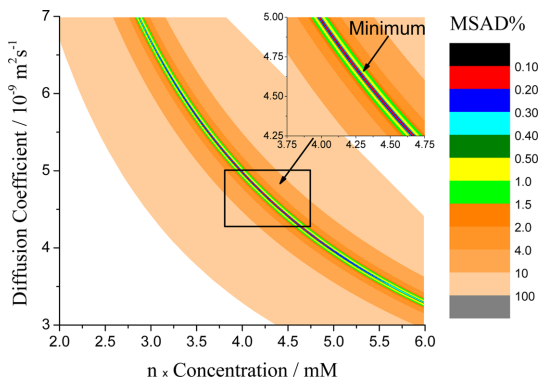

Fig. 3. The two-dimensional contour plot of mean scaled absolute deviation (MSAD), where x axis corresponds to the product of concentration and the number of electron transferred, and y axis corresponds to the diffusion coefficient of O_2 in air-equilibrated EtOH/0.1 M TBACl solution. The scale of MSAD is listed on the right. This is obtained from the chronoamperometry for the reduction of O_2 at a transient time of 0.5s.

Table 1. Parameters used in the EC' simulation model. All data were obtained from experimental results in electrolytic ethanol solution within this work

Parameters	Values
Concentration of O_2 in air-equilibrated EtOH (mM)	2.13 ± 0.20
Solubility of pure O_2 (mM)	10.14 ± 0.95
$C_{MV^{2+}}$ (mM)	1.00
D_{O_2} ($\times 10^{-6}$ cm^2 s^{-1})	47.0 ± 4.1
$D_{MV^{2+}}$ ($\times 10^{-6}$ cm^2 s^{-1})	4.65 ± 0.04
k_0 (cm s^{-1})	1
$E_{MV^{2+/\bullet+}}$	−0.352 V (*vs.* Ag/AgCl – 1 M KCl)
$\alpha_{MV^{2+}}$	0.79

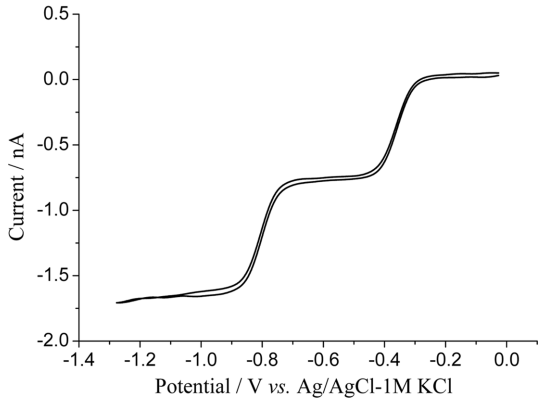

Fig. 4. Cyclic voltammogram for the two 1-electron redox of 1 mM MV^{2+} in a N_2 saturated EtOH/0.1 M TBACl solution on a μ-C electrode at 25 mV s^{-1}.

in an air-equilibriated EtOH were evaluated, by taking the mean of four sets of data with lowest MSAD %, to be $(4.70 \pm 0.41) \times 10^{-5}$ cm^2 s^{-1} and (4.25 ± 0.39) mM respectively. The optimum fitting of simulated result is also shown in Fig. 2 (circle). The experimentally obtained diffusion coefficient is found to be comparable with the literature. Values for D_{O_2} range from $(1.64 - 4.0) \times 10^{-5}$ cm^2 s^{-1}, despite the fact that all previously reported experiments were in the absence of supporting electrolyte.[23-26] To the best of the authors' knowledge, it is the first time that D_{O_2} is determined in an electrolytic EtOH solution. Moreover, the concentration of O_2 in air-equilibriated EtOH can be determined by the evaluation of *n*, the number of electrons involved in the I_{ss}. The electrochemical reduction of O_2 demonstrates one to four electron transfers, dependent on conditions such as solvent media and electrode materials.[22,27-29] However, the number of electrons transferred in electrolytic EtOH solution has not yet been identified. The value of *n* herein could be 1, 2, or 4. Che *et al.* reported the solubility of O_2 in pure EtOH being 10.04 mM.[13] Therefore, knowing that air contains 21% of O_2,[30,31] only the value of *n* being 2 gives the most sensible C_{O_2} in electrolytic EtOH solution, *i.e.* (10.14 ± 1.00) mM. Both values of C_{O_2} and D_{O_2}, as given in Table 1, are utilised later in the simulation for MV^{2+} mediated O_2 reduction.

3.2 MV^{2+} redox responses and kinetics

Before further elaboration of mediated redox response of MV^{2+} upon O_2 reduction, the MV^{2+} redox reaction in the absence of oxygen is first investigated.

The 1.00 mM MV^{2+} electrochemical responses were carried out in N_2 saturated EtOH solution supported with 0.1 M TBACl salt on a μ-C electrode. The two 1-electron redox signal was first obtained at 25 mV s^{-1} and is shown in Fig. 4. Two steady-state currents were achieved, corresponding to the first and second electron reduction of MV^{2+} to form $MV^{\bullet+}$ and MV^0 respectively. Similar responses were also reported in other solvents, namely dimethyl sulfoxide[4], dimethylformamide[5] and aqueous systems (Fig. 7).[6,8] These two electron transfers are well separated by over 200 mV. As a result, at lower overpotentials there is substantial amount of radical cations produced, which are able to diffuse away from the electrode surface and participate in the electrocatalysis. The electrocatalytic mechanism herein is focused mainly on the mediator couple of $MV^{2+/\bullet+}$.

Accordingly the first electron reduction of MV^{2+} is studied. Cyclic voltammetries were recorded on a μ-C electrode at variable scan rates ranging from 5 to 1000 mV s^{-1}, shown in Fig. 5 (line). The diffusion coefficient of MV^{2+} in EtOH supported with 0.1 M TBACl solution can be calculated from Eqn. (1) *via* I_{ss} at low scan rate (5 mV s^{-1}). A value of $(4.65 \pm 0.04) \times 10^{-6}$ cm^2 s^{-1} was obtained. The transfer coefficient, α, can be obtained from a Tafel plot. A representative Tafel plot is shown as inset in Fig. 5(a) at 5 mV s^{-1}, and the corresponding α value is 0.79. $E_{MV^{2+/\bullet+}}$ in EtOH solution is assumed to be the same as the half-wave potential, being −0.352 V (*vs.* Ag/AgCl – 1 M KCl).

Utilising all the parameters obtained above, the heterogeneous electron transfer rate constant (k_0) can be

obtained by a microdisc simulation model developed by Klymenko (Section 2.3).[20] The simulated CVs were optimized by fitting both the wave shape and I_{ss} at scan range from 5 to 1000 mV s^{-1}. The fitted data are shown in Fig.5 at 5, 100, and 1000 mV s^{-1}. It can be seen that as scan rate increases, the convergent diffusional regime gradually switches to linear diffusion due to the reduced experimental time scale. Note that the experimental CVs were blank subtracted and baseline corrected. Excellent agreement is achieved between experimental and simulated results. The simulated CVs become unchanged when $k_0 \geq 1$ cm s^{-1}.

After having obtained the parameters for both MV^{2+} and O_2 necessary for the simulations reported below, the mediated responses are now further discussed.

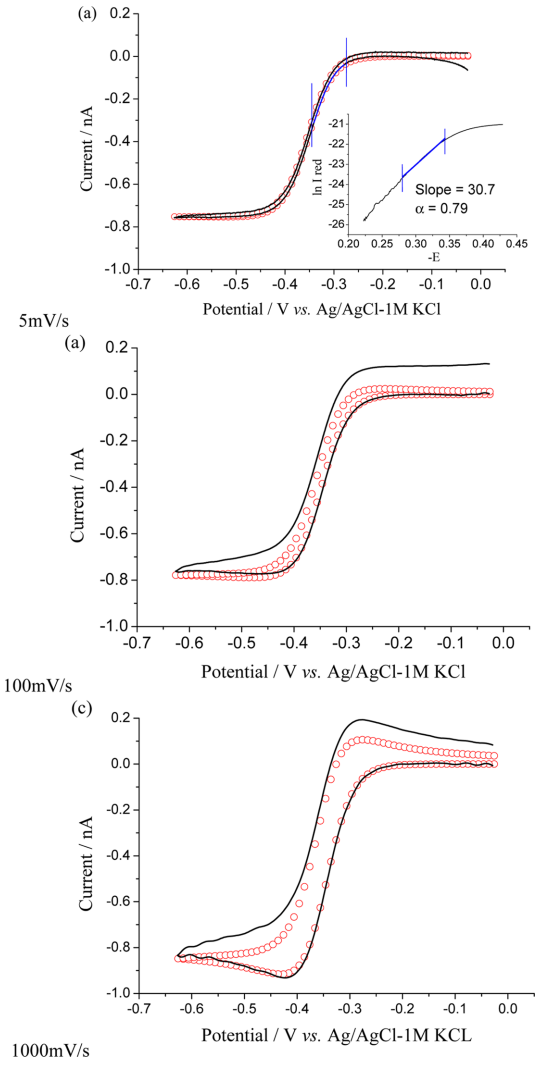

Fig. 5. The experimental (line) and simulated (circle) cyclic voltammograms for the 1-electron transfer of 1 mM MV^{2+} in a N_2 saturated EtOH/0.1 M TBACl solution on a μ-C electrode at scan rates of (a) 5 mV s^{-1} (The forward scan highlighted in blue was selected as Tafel analysis region. Inset is the Tafel plot of á being 0.788); (b) 100 mV s^{-1}; (c) 1000 mV s^{-1}.

3.3 The MV^{2+} mediated O_2 reduction

The electrocatalytic (or EC') mechanism of MV^{2+} mediated O_2 reduction is proposed as following,

$$MV^{2+} + e^- \overset{k_0}{\leftrightarrow} MV^{\bullet+} \quad E_{MV^{2+/\bullet+}} \tag{1}$$

$$MV^{\bullet+} + O_2 \overset{k_f}{\rightarrow} MV^{2+} + O_2^{\bullet-} \tag{2}$$

where $E_{MV^{2+/\bullet+}}$ is the formal potential of $MV^{2+/\bullet+}$ redox couple, k_0 is the heterogeneous electron transfer rate constant (cm s^{-1}), and k_f is the homogeneous rate of electron transfer (mol^{-1} dm^3 s^{-1}). In the EC' mechanism, MV^{2+} acts as the mediator to reduce O_2 to superoxide ($O_2^{\bullet-}$), *via* reduction to $MV^{\bullet+}$.

First, the electrocatalytic response of O_2 reduction in an air-equilibrated EtOH solution supported with 0.1 M TBACl on a boron-doped diamond (BDD) macroelectrode is shown in Fig. 6. The cyclic voltammogram of MV^{2+} reduction in N_2 saturated solution represents two 1-electron reduction waves. The direct O_2 reduction only takes place at high overpotentials. An electrocatalytic peak at –0.71 V corresponds to the $MV^{\bullet+}$ mediated O_2 reduction. There is a second reductive wave at *ca.* –1.0 V at the electrocatalytic diffu-

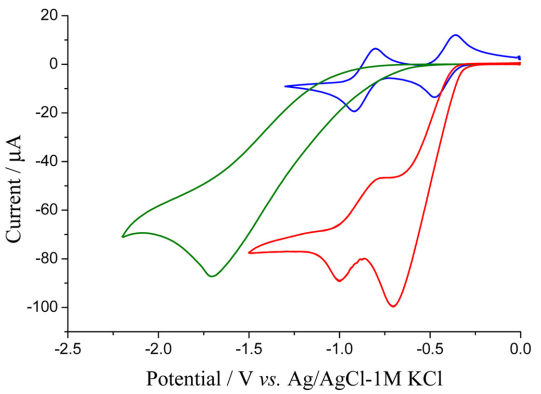

Fig. 6. Comparison of cyclic voltammograms in EtOH/0.1 M TBACl solution on a BDD electrode at 100 mV s^{-1}. Blue: two 1-electron transfer waves of 1 mM MV^{2+} in N_2 saturated solution; Green: direct reduction of O_2 in air-equilibrated solution; Red: 1 mM MV^{2+} mediated O_2 reduction in air-equilibrated solution.

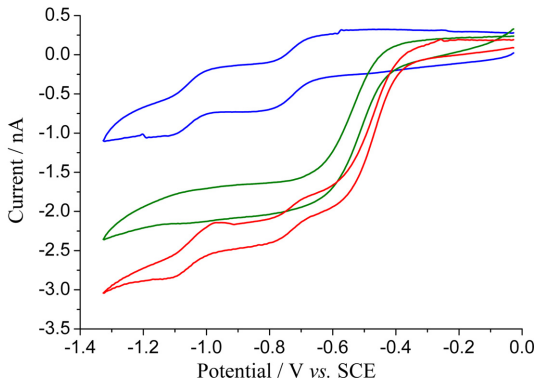

Fig. 7. Comparison of cyclic voltammograms in aqueous PBS/ 0.1 M KCl (pH 6.7) on a μ-C electrode at 25 mV s^{-1}. Blue: two 1-electron transfer waves of 1 mM MV^{2+} in N_2 saturated PBS; Green: direct reduction of O_2 in air-equilibrated PBS; Red: presence of both 1 mM MV^{2+} and air O_2.

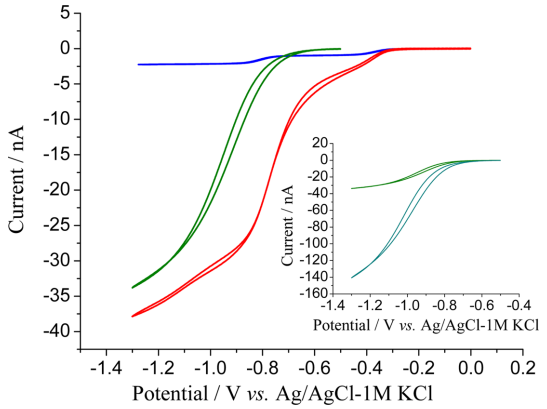

Fig. 8. Comparison of cyclic voltammograms in EtOH/ 0.1 M TBACl solution on a μ-C electrode at 100 mV s^{-1}. Blue: two 1-electron transfer waves of 1 mM MV^{2+} in N_2 saturated solution, Green: direct reduction of O_2 in an air-equilibrated solution; Red: 1 mM MV^{2+} mediated O_2 reduction in air-equilibrated solution. Inset depicts the direct reduction of O_2 in air-equilibrated (green) and O_2-saturated (cyan) EtOH solution.

sional current tail. It may correlate to further mediated reduction related to the di-reduced viologen intermediate species. However, the overlap between the $MV^{\bullet+/0}$ redox response and direct O_2 reduction complicates any definitive analysis upon gaining electrocatalytic kinetics information. Therefore, the following study in ethanolic solution is mainly focused on the radical cation mediated O_2 reduction.

The voltammetric responses in the presence of both MV^{2+} and O_2 on a μ-C electrode are markedly different in aqueous solution as compared to that is in EtOH solution. Fig. 7 shows the same redox couples in aqueous phosphorous buffer solution (PBS, pH 6.7) supported with 0.1 M potassium chloride on a μ-C electrode. The cyclic voltammograms demonstrate 1.00 mM MV^{2+} redox only, O_2 direct reduction, and MV^{2+} redox in the presence of O_2, The consecutive 2-electron reduction I_{ss} waves are clearly shown for redox couples of $MV^{2+/\bullet+}$ and $MV^{\bullet+/0}$. The direct O_2 reduction commences at *ca.* 300 mV more positive in potential as compared to the first electron transfer of MV^{2+}. Unsurprisingly, when combining both redox species in the aqueous solution, *no* electrocatalytic response is seen (Fig. 7 red wave). The three redox waves correlate to the O_2/H_2O_2, $MV^{2+/\bullet+}$ and $MV^{\bullet+/0}$ responses. In order to achieve a favourable homogeneous electron transfer process (Eqn. (2)), the formal potential of $O_2/O_2^{\bullet-}$ should be at more positive potential as compared to that of the $MV^{2+/\bullet+}$ redox couple. Knowing the $E_{O_2/O_2^{\bullet-}}$ of –0.4212 V and $E_{MV^{2+/\bullet+}}$ of –0.7055 V in aqueous solution *vs.* standard calomel electrode (SCE),[6,32] the homogeneous electron transfer process (Eqn. (2)) is expected to be thermodynamically favourable. However, the direct O_2 reduction takes place with much lower driving force. Therefore, no electrocatalytic reduction is seen on μ-C electrode. Note that the mediated reduction in aqueous solution was previously seen on BDD and glassy carbon electrodes for both dissolved and surface bound viologen.[6,33] The fact that the $E_{O_2/O_2^{\bullet-}}$ exhibits a much more positive potential in water than in anhydrous solvents as against $E_{MV^{2+/\bullet+}}$ is presumably related to the stronger solvation of $O_2^{\bullet-}$ by water as compared with organic solvents.

Fig. 8 shows the corresponding cyclic voltammograms at a scan rate of 25 mV s^{-1} for 1.00 mM MV^{2+} mediated O_2 reduction signal, direct 2-electron MV^{2+} redox and direct 2-electron air O_2 redox, respectively, where the inset shows a comparison of direct O_2 reduction in both air-equilibrated and pure O_2-saturated EtOH solution. It is evident that within the region of the first electron reduction of $MV^{2+/\bullet+}$ ($E_{MV^{2+/\bullet+}}$ is –0.352 V) there is no heterogeneous current contribution from O_2 reduction, where the latter only occurs after *ca.* –0.6 V. Therefore, on the mediated signal response the current contribution prior to –0.6 V accounts for the electrocatalytic reduction of O_2 via $MV^{\bullet+}$ intermediate species (Eqn. (2)), and beyond –0.6 V the background current contribution is mainly from direct O_2 reduction.

The important feature of zero-current from heterogeneous O_2 reduction on a μ-C electrode enables an unambiguous study of the electrocatalytic process of MV^{2+} mediated O_2 reduction. An attempt to study the homogeneous step is carried out here. The proposed EC' mechanism was modelled *via* an in-house developed program by Ward *et al.* (Section 2.3)[21]. Parameters used in simulation, such as concentration of O_2 in air-equilibrated EtOH, C_{O_2}, D_{O_2}, $C_{MV^{2+}}$, $D_{MV^{2+}}$, k_0, $E_{MV^{2+/\bullet+}}$ and $\alpha_{MV^{2+}}$ are tabulated in Table 1. $MV^{\bullet+}$ is assumed to have the same diffusion coefficient as MV^{2+}, and $O_2^{\bullet-}$ is assumed to have the same diffusion coefficient as O_2. By utilising the simple EC' mechanism, the model was optimized to give a best fit by considering both the wave shape and steady-state current.

The air-equilibrated response was first simulated. Fig. 9 depicts both the experimental (Line) and simulated (Circle) data of electrocatalytic responses of O_2 reduction in an air-equilibrated EtOH solution. An excellent correlation of experimental and simulated results is shown at *ca.* −0.4 V. The resulting homogeneous rate of electron transfer (k_f) is $(1 \pm 0.1) \times 10^5$ mol^{-1} dm^3 s^{-1}. If taking Eqn. (1) and known the concentration of O_2 and D_{O_2} for 2-electron reduction of O_2, the estimated I_{ss} for complete reduction is about 15 nA. It is in contrast to the experimentally obtained I_{ss} of *ca.* 2.5 nA. Hence, it can be concluded that the homogeneous electron transfer step (Eqn. (2)) is the rate determining step. This was further proved via simulation by increasing k_f until 1×10^8 mol^{-1} dm^3 s^{-1} when current limits at about 15 nA (not shown). Moreover, the much smaller I_{ss} suggests that only partial catalysis is achieved. As previously discussed, in an aqueous system the concentration ratio of the mediator against O_2 can directly relate to a switch between partial catalysis to 'total catalysis'.[6] By increasing this concentration ratio, it is predicted that the partial catalysis can also be tuned towards the 'total catalysis' regime.[6,34,35] This can be further proved via simulation by increasing the concentration of MV^{2+} from 1 mM to 4, 6, 8 and 10 mM (Fig. 9), keeping the concentration of O_2 unchanged. As the concentration of MV^{2+} approaches *ca.* 8 mM the I_{ss} limits at about 15 nA. Oxygen reduction 'total catalysis' now takes place. The same parameter of k_f being 1×10^5 mol^{-1} dm^3 s^{-1} is then used to simulate the O_2-saturated case, shown in Fig. 9 inset. Again, a good agreement was achieved.

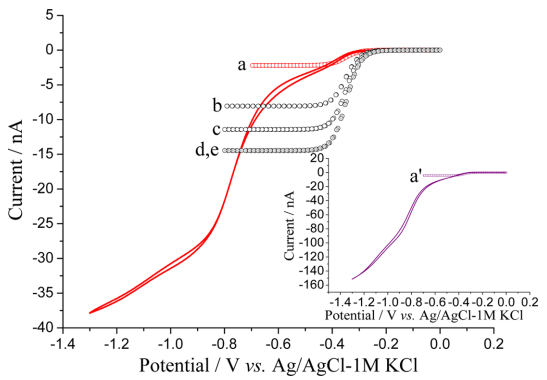

Fig. 9. The experimental (line, 1 mM MV^{2+}) and simulated (circle, various concentration of MV^{2+}) steady state currents of MV^{2+} mediated O_2 reduction in both air-equilibrated (red) and O_2-saturated (purple, inset) EtOH / 0.1 M TBACl solution on a ì-C electrode at 100 mV s^{-1}. (a) and (a') 1 mM MV^{2+}; (b) 4 mM MV^{2+}; (c) 6 mM MV^{2+}; (d) 8 mM MV^{2+}; (e, smaller circle) 10mM MV^{2+}, where k_f is 1×10^5 M^{-1} s^{-1} for all simulations.

Moreover, it is of interest to note that there is an elevation after the predicted steady-state currents for both air-equilibrated and O_2-saturated cases. This is likely due to the migration current in the presence of MV^{2+} molecules. As migration of MV^{2+} molecules requires an electric field, the potential of zero charge (PZC) for the μ-C electrode was estimated, and a migration current would be observed at more negative potential than PZC. Moreover, under the studied conditions, the low dielectric constant of ethanol ($\varepsilon_{EtOH} = 24.6$) [36] compared to water ($\varepsilon_{H_2O} = 78.4$) or acetonitrile ($\varepsilon_{CH_3CN} = 36.0$)[37] is suggested to lead to a more significant migration contribution.

Information about the PZC comes from the investigation of interfacial capacitance at low concentrations of supporting electrolyte.[38] The specific capacitance of the system was estimated by cyclic voltammetry as a function of potential, in an EtOH solution supported with only 1.00 mM TBACl. Each cyclic voltammogram was recorded over a limited potential range of 50 mV at a high scan rate of 2 V s^{-1}, shown in Fig. 10. The difference in current between the forward and backward scan (I_{cap}, *Amp*) can be correlated to the specific capacitance of the electrode (C_{sp}, $\mu F \bullet cm^{-2}$) by the following equation:

$$I_{cap} = 2\,\nu C_{DL} \qquad (7)$$

where $C_{DL} = A \times C_{sp}$. Parameters are defined as ν being the scan rate (V s^{-1}), C_{DL} being the double layer capacitance (μF) and A being the area of the electrode surface (cm^2). Hence, given the measured I_{cap} and A, C_{sp}

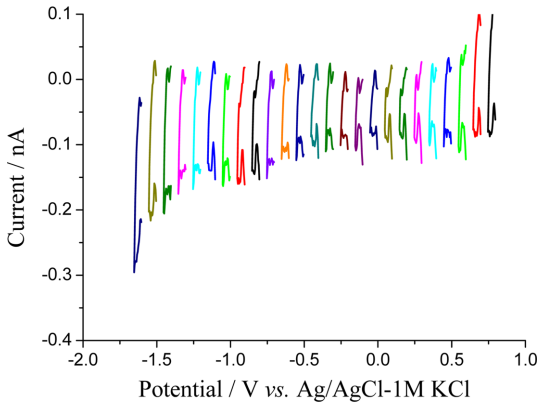

Fig. 10. Cyclic voltammograms of blank scans in N_2 saturated EtOH supported with only 1 mM TBACl over a limited potential range of 50 mV at a high scan rate of 2 V s^{-1} at a μ-C electrode.

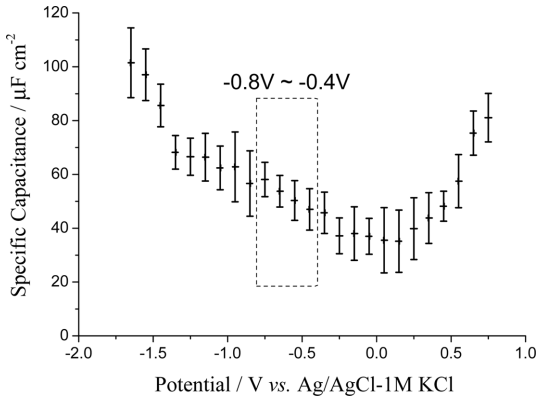

Fig. 11. The variation of specific capacitance for a μ-C electrode as a function of potential in N_2 saturated EtOH/1 mM TBACl solution.

can be plotted in Fig. 11. The distinct minimum observed at *ca.* 0 V likely corresponds to the PZC.[39-41] A significant increase in C_{sp} is observed specifically when the potential becomes more negative than –0.4 V. It suggests that at potentials negative of the PZC, the charged molecules are inclined to be attracted towards the electrode surface. The boxed region can account for the difference in current in the corresponding potential range between experimental and simulated voltammograms. This migration contribution, in fact, is arguably useful because it is enhancing the mass transport again over above diffusion in electrocatalytic O_2 reduction. It should be noted that migration effects are only apparent for the mediated and not the MV^{2+} only reduction. This likely arises due to the relatively small size of the reaction layer under electrocatalysis as compared to the unperturbed diffusion layer in the absence of O_2. Upon contraction of the reaction layer to dimensions comparable to that of the electric field the mass transport of the positively charged MV^{2+} towards the electrode will be increased. This greater mass transport may result in the observed potential dependent enhancement of the electrocatalytic responses.

4. Conclusions

The study of oxygen reduction in ethanol systems is of significant importance due to the higher oxygen solubility in this solvent as compared to aqueous environments. Hence, this may prove to be a beneficial route towards the electrochemical synthesis of hydrogen peroxide. The present work has been focussed upon the study of the mediated oxygen reduction in ethanol solution. However, the thermodynamics, kinetics and mass transport of the electrochemical system are significantly altered as compared to that of aqueous environment. To the best knowledge of the authors, it is the first time that these data are obtained electrochemically in an electrolytic ethanol solution. The diffusion coefficient and solubility of oxygen were determined *via* chronoamperometry using Shoup and Szabo analysis and mean scaled absolute deviation method in an electrolytic ethanol solution to be $(4.70 \pm 0.41) \times 10^{-5}$ $cm^2\ s^{-1}$ and (10.14 ± 1.00) mM. The number of electrons involved in the first steady-state current was evaluated to be 2, showing H_2O_2 to be the reaction product. Moreover, the diffusion coefficient of methyl viologen was obtained from the steady-state current, being $(4.65 \pm 0.04) \times 10^{-6}$ $cm^2\ s^{-1}$. Fast electrode kinetics was shown by simulation fitting. The heterogeneous electron transfer rate constant is $k_0 \geq 1$ cm s^{-1} with the obtained transfer coefficient of 0.79.

For the first time methyl viologen mediated oxygen reduction in ethanol has been proved to be feasible via both boron-doped diamond and micro-carbon disc electrodes. The electrocatalytic response is demonstrated to be mainly contributed from the radical cation, $MV^{\bullet+}$, mediated oxygen reduction. Successful modelling of the experimental data results in a homogeneous rate constant (k_f) of $(1 \pm 0.1) \times 10^5$ $M^{-1}\ s^{-1}$, of which step was shown to be the rate determining step. Under the studied experimental conditions, only partial catalysis was obtained. With the aid of simulation program, it can be seen that by increasing the concentration ratio of MV^{2+} to O_2 a 'total catalysis' regime can be achieved. Moreover, a potential dependent electrocatalytic steady-state current is likely

resulted from the migration current contribution, which can be arguably useful because it is enhancing the mass transport again over above diffusion in electrocatalytic O_2 reduction.

References

1. C. L. Bird and A. T. Kuhn, *Chem. Soc. Rev.*, 1981, **10**, 49-82.
2. K. Tanabe, T. Yasuda, M. Yoshio and T. Kato, *Org. Lett.*, 2007, **9**, 4271-4274.
3. P. M. S. Monk, R. D. Fairweather, M. D. Ingram and J. A. Duffy, *J. Chem. Soc., Perkin Transactions 2*, 1992, 2039-2041.
4. C. P. Andrieux, P. Hapiot and J. M. Savéant, *J. Electroanal. Chem.*, 1985, **189**, 121-133.
5. I. V. Shelepin and O. A. Ushakov, *Zh. Fiz. Khim.*, 1973, **49**.
6. Q. Lin, Q. Li, C. Batchelor-McAuley and R. G. Compton, *Phys. Chem. Chem. Phys.*, 2013, **15**, 7760-7767.
7. R. N. F. Thorneley, *Biochim. Biophys. Acta*, 1974, **333**, 487-496.
8. J. A. Farrington, M. Ebert, E. J. Land and K. Fletcher, *Biochim. Biophys. Acta*, 1973, **314**, 372-381.
9. I. Fridovich and H. M. Hassan, *Trends Biochem. Sci*, 1979, **4**, 113-115.
10. J. M. Campos-Martin, G. Blanco-Brieva and J. L. G. Fierro, *Angew. Chem. Int. Ed.*, 2006, **45**, 6962-6984.
11. I. Yamanaka and T. Murayama, *Angew. Chem. Int. Ed.*, 2008, **47**, 1900-1902.
12. J. K. Edwards, B. Solsona, E. N. N, A. F. Carley, A. A. Herzing, C. J. Kiely and G. J. Hutchings, *Science*, 2009, **323**, 1037-1041.
13. Y. Che, K. Tokuda and T. Ohsaka, *Bull. Chem. Soc. Jpn.*, 1998, **71**, 651-656.
14. Y. Wang, E. I. Rogers and R. G. Compton, *J. Electroanal. Chem.*, 2010, **648**, 15-19.
15. Y. Saito, Rev. Pola., 1968, **15**, 178-187
16. C. A. Paddon, D. S. Silvester, F. L. Bhatti, T. J. Donohoe and R. G. Compton, *Electroanalysis*, 2007, **19**, 11-22.
17. L. Xiong, L. Aldous, M. C. Henstridge and R. G. Compton, *Anal. Methods*, 2012, **4**, 371-376.
18. O. V. Klymenko, R. G. Evans, C. Hardacre, I. B. Svir and R. G. Compton, *J. Electroanal. Chem.*, 2004, **571**, 211-221.
19. D. Shoup and A. Szabo, *J. Electroanal. Chem.* , 1982, **140**, 237-245.
20. N. V. Rees, O. V. Klymenko, R. G. Compton and M. Oyama, *J. Electroanal. Chem.*, 2002, **531**, 33-42.
21. K. R. Ward, N. S. Lawrence, R. S. Hartshorne and R. G. Compton, *J. Phys. Chem. C*, 2011, **115**, 11204-11215.
22. D. T. Sawyer, A. Sobkowiak and J. J. L. Roberts, *Electrochemistry for Chemists*, John Wiley and Sons, Inc1995.
23. E. Sada, S. Kito, T. Oda and Y. Ito, *Chem. Eng. J.*, 1975, **10**, 155-159.
24. I. M. Krieger, G. W. Mulholland and C. S. Dickey, *J. Phys. Chem.*, 1967, **71**, 1123-1129.
25. W. R. Ware, *J. Phys. Chem.*, 1962, **66**, 455-458.
26. P. Chang and C. R. Wilke, *The Journal of Physical Chemistry*, 1955, **59**, 592-596.
27. Q. Li, C. Batchelor-McAuley, N. S. Lawrence, R. S. Hartshorne and R. G. Compton, *J. Electroanal. Chem.*, 2013, **688**, 328-335.
28. J. Fei Wu, Y. Che, T. Okajima, F. Matsumoto, K. Tokuda and T. Ohsaka, *Electrochim. Acta*, 1999, **45**, 987-991.
29. D. Vasudevan and H. Wendt, *J. Electroanal. Chem.*, 1995, **392**, 69-74.
30. D. J. Jacob, *Introduction to Atmospheric Chemistry*, Princeton University Press, Princeton, N.J.,, 1999.
31. I. N. Levine, *Physical Chemistry*, McGraw-Hil, Boston, 2009.
32. W. Koppenol;, D. Stanbury; and P.Bounds, *Free Radical Bio. Med.*, 2010, **49**, 317-322.
33. C.-W. Lee and J.-M. Jang, *Bull. Korean Chem. Soc.*, 1994, 15, 563-567.
34. J.-M. Savéant, *Elements of Molecular and Biomolecular Electrochemistry*, John Wiley & Sons, Inc., Hoboken, New Jersey, 2006.
35. J.-M. Savéant, *Chem. Rev.*, 2008, **108**, 2348-2378.
36. G. E. Papanastasiou and I. I. Ziogas, *J. Chem. Eng. Data*, 1991, **36**, 46-51.
37. G. P. Cunningham, G. A. Vidulich and R. L. Kay, *Journal of Chemical & Engineering Data*, 1967, **12**, 336-337.
38. A. J. Bard and L. R. Faulkner, *Electrochemical methods: Fundamentals and Applications*, Wiley & Sons, New York, 2001.
39. R. Nissim, C. Batchelor-McAuley, M. C. Henstridge and R. G. Compton, *Chem. Commun.*, 2012, **48**, 3294-3296.
40. M. Hahn, M. Baertschi, O. Barbieri, J. C. Sauter, R. Kötz and R. Gallay, *Electrochem. Solid-State Lett.*, 2004, **7**, A33-A36.
41. H. Gerischer, R. McIntyre, D. Scherson and W. Storck, *J. Phys. Chem.*, 1987, **91**, 1930-1935.